

Formation, Isomerization, and Dissociation of α -Carbon-Centered and π -Centered Glycylglycyltryptophan Radical Cations

Dominic C. M. Ng,^{†,‡} Tao Song,^{†,‡} S. O. Siu,[†] C. K. Siu,[§] Julia Laskin,^{||} and Ivan K. Chu*,[†]

Department of Chemistry, The University of Hong Kong, Pokfulam Road, Hong Kong, China, Pacific Northwest National Laboratory, Fundamental Sciences Division, Richland, Washington, and Department of Biology and Chemistry, City University of Hong Kong, Tat Chee Avenue, Kowloon, Hong Kong, China

Received: September 5, 2009; Revised Manuscript Received: December 19, 2009

Gas phase fragmentations of two isomeric radical cationic tripeptides of glycylglycyltryptophan—[G \cdot GW]⁺ and [GGW] \cdot ⁺—with well-defined initial radical sites at the α -carbon atom and the 3-methylindole ring, respectively, have been studied using collision-induced dissociation (CID), density functional theory (DFT), and Rice–Ramsperger–Kassel–Marcus (RRKM) theory. Substantially different low-energy CID spectra were obtained for these two isomeric GGW structures, suggesting that they did not interconvert on the time scale of these experiments. DFT and RRKM calculations were used to investigate the influence of the kinetics, stabilities, and locations of the radicals on the competition between the isomerization and dissociation channels. The calculated isomerization barrier between the GGW radical cations (>35.4 kcal/mol) was slightly higher than the barrier for competitive dissociation of these species (<30.5 kcal/mol); the corresponding microcanonical rate constants for isomerization obtained from RRKM calculations were all considerably lower than the dissociation rates at all internal energies. Thus, interconversion between the GGW isomers examined in this study cannot compete with their fragmentations.

Introduction

Peptide and protein radicals derived from copper(II)–protein complex ions are key intermediates in both Alzheimer’s disease (β -amyloid peptide) and bovine spongiform encephalitis (prion protein).^{1,2} α -Carbon-centered radicals on peptide backbones presumably play major roles in many oxidative processes within cells, such as selective cleavage leading to protein damage. Dissociations of radical peptides and proteins can proceed through a number of important chemical processes: hydrogen atom abstraction, fragmentation, isomerization, rearrangement, and electron transfer.^{3–5} Gas phase fragmentation of radical peptide species provides important information on the competition between these processes in the absence of solvent.

Gas phase dissociation of odd-electron radical peptide cations has attracted considerable attention, partly because several novel sequencing approaches—including electron capture dissociation (ECD)^{6,7} and electron transfer dissociation (ETD)^{8,9}—rely on fragmentation of radicals. Classical M $^+$ radical cations comprise another class of odd-electron peptide ions that can be produced in the gas phase. Several approaches have been developed for the formation of M $^+$ peptide ions: collision-induced dissociation (CID) of transition metal/peptide complexes,^{10–12} high-energy collisional excitation with a target gas to induce electron transfer in an accelerator mass spectrometer,¹³ multiphoton laser desorption ionization of nonvolatile small peptides that contain aromatic chromophores,¹⁴ CID of peptides derivatized with a conjugated free radical initiator¹⁵ or other labile radical precursors,¹⁶ laser photolysis of peptides containing photolabile tags,¹⁷

and photodissociation of protonated peptides at a wavelength of 157 nm.¹⁸

Several recent studies have focused on the fragmentations of model molecular radical cations—containing aliphatic, aromatic, and basic amino acid residues—using tandem mass spectrometry and theoretical DFT calculations.^{19–40} A mechanism involving charge-directed fragmentation and featuring a “mobile proton” has been used to explain the dissociation of tripeptide radical cations.⁴³ The calculated lowest-energy isomer of the radical cation of glycylglycylglycine has a captodative structure with the radical center located on the N-terminal α -carbon. The locations of both the charge and the radical are critical factors determining the fragmentation pathways. Indeed, the competitive radical- and charge-induced dissociations of radical peptides bound to alkaline metal ions, such as sodium and lithium ions, are extremely metal-specific.^{41,42} O’Hair and co-workers presented a detailed discussion of the radical-initiated dissociations of a variety of small glycine-containing peptides possessing fixed charge; they also demonstrated that isomers of sodiated serine nitrate ester derivatives with predetermined radical sites readily interconvert through 1,4-hydrogen atom migration.⁴¹ In contrast, Wesdemiotis and co-workers reported that lithiated and dilithiated forms of α -dipeptide radical cationic isomers are not interconvertible.⁴²

Comprehensive studies of the roles played by the radical sites have been hindered by difficulties in generating peptide radical cations featuring initial radical sites located at well-defined positions. α -Centered radical cationic peptides are ideal systems for studying the fundamental parameters that govern dissociation and isomerization of peptide radical cations. A recent report described the dissociations of isomeric radicals of triglycine—[G \cdot GG]⁺, [GG \cdot G]⁺, and [GGG \cdot]⁺—with well-defined initial radical sites at different α -carbon atoms in the peptide.^{43,44} Such radical species were produced through multiple-stage CID of [Cu II (L)(M)] $^{2+}$ complexes (where L is an auxiliary ligand and

* To whom correspondence should be addressed. E-mail: ivankchu@hku.hk.

[†] The University of Hong Kong.

[‡] Contributed equally to this work.

[§] City University of Hong Kong.

^{||} Pacific Northwest National Laboratory.

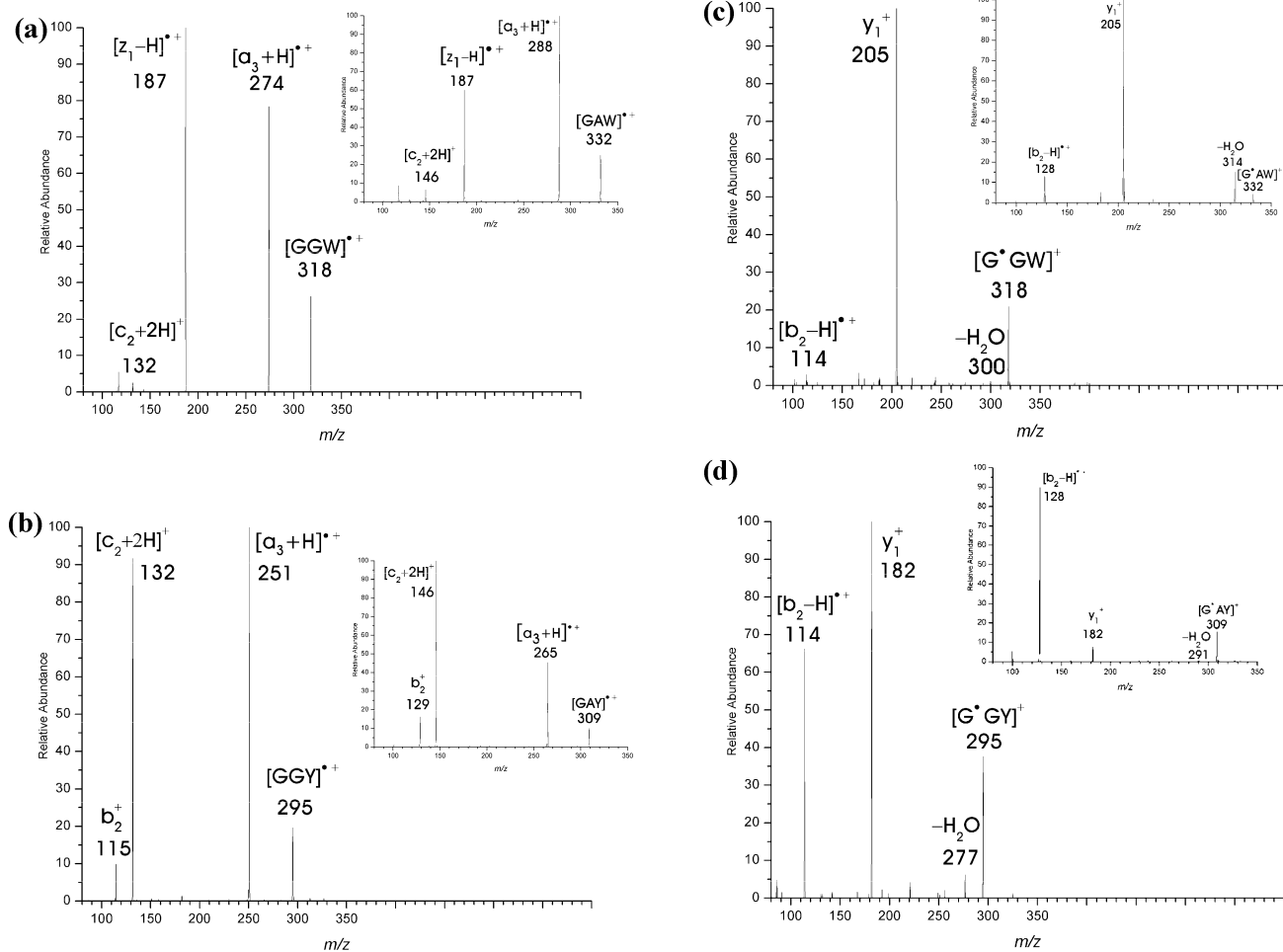


Figure 1. CID spectra of (a) $[GGW]^{•+}$ (inset: $[GAW]^{•+}$), (b) $[GGY]^{•+}$ (inset: $[GAY]^{•+}$), (c) $[G^{•}GW]^{•+}$ (inset: $[G^{•}AW]^{•+}$), and (d) $[G^{•}GY]^{•+}$ (inset: $[G^{•}AY]^{•+}$).

M is YGG, GYG, or GGY). The barriers for interconversion among the triglycine isomers (≥ 44.7 kcal/mol) are significantly higher than those for the tautomerism of protonated triglycine isomers (< 17 kcal/mol).^{43,45} These high energy barriers result in slow interconversion among the different isomers of the GGG radical cation; the observation of different dissociation products from the isomeric species clearly demonstrates the importance of defining the initial radical site in the $M^{•+}$ species.

Before we began this study, nonconvertible α -centered radical isomers with well-defined initial radical sites had been reported experimentally only for the sodiated amino acids,⁴¹ lithiated/dilithiated dipeptides,⁴² and aliphatic tripeptide GGG^{43,44} but not for aromatic tripeptides. Peptides containing aromatic residues (Tyr, Typ, His, Phe) can form various types of radical cations, including π -radical, benzylic, α -radical, and carboxy radical cations.⁴⁰ The proton affinities and ionization energies of the amino acid side chains could presumably also play significant roles in selecting between the competitive reactions. Although DFT calculations predict an absence of interconversion between the α -carbon-centered radical and π -radical of the aromatic tryptophan cation,^{10,19,40} the experimental formation and isomerization of such isomeric cations remains unconfirmed.

In this present study, we extended our investigation to the experimental generation of noninterconverting radical cationic glycylglycyltryptophan (GGW) isomers, featuring an aromatic side chain, in an effort to further investigate how the kinetics, stabilities, and locations of the radicals influence the competition between the isomerization and dissociation channels. We formed

and examined two noninterconverting radical cationic isomeric pairs— $[G^{•}GW]^{•+}/[GGW]^{•+}$ and $[G^{•}GY]^{•+}/[GGY]^{•+}$ —and accounted for the kinetics of their different dissociation pathways using statistical theories and Rice–Ramsperger–Kassel–Marcus (RRKM) modeling. The isomeric π -radical cation $[GGW]^{•+}$ and the α -centered radical cation $[G^{•}GW]^{•+}$ were good candidates for our experimental investigations because (i) the low ionization energy of the tryptophanyl residue (ca. 8.8 eV)⁴⁶ delocalizes the radical site and (ii) the generation of the distonic radical cation $[GGW]^{•+}$, with the radical theoretically located on the 3-methylindole ring, has been reported previously.¹⁹ In recent studies of isomeric His^{•+},^{20b} infrared multiple photon dissociation (IRMPD) provided the first strong complementary evidence to support the predicted (DFT) calculations of the lowest-energy structure among five calculated His^{•+} structures; IRMPD revealed that the distonic captodative α -centered radical structure (-31.4 kcal/mol) is the long-lived observable ion, not the canonical form (0 kcal/mol) in which the radical and charge are delocalized on the aromatic ring. The low energy barrier for interconversion (8.4 kcal/mol) allows the canonical His^{•+} species to rapidly isomerize to the distonic captodative α -centered radical structure.⁴⁷ Similarly, DFT calculations on the radical cations of *N*-acetyltryptophan methyl ester $[AcWOME]^{•+}$ and *N*-acetylyrosine methyl ester $[AcYOME]^{•+}$ revealed that the lowest-energy structures of both radical cations also involve π -radicals, but in each case, the energy required for hydrogen atom migration of the transition structure from the α -carbon atom to the amide oxygen atom was greater than 30 kcal/mol,

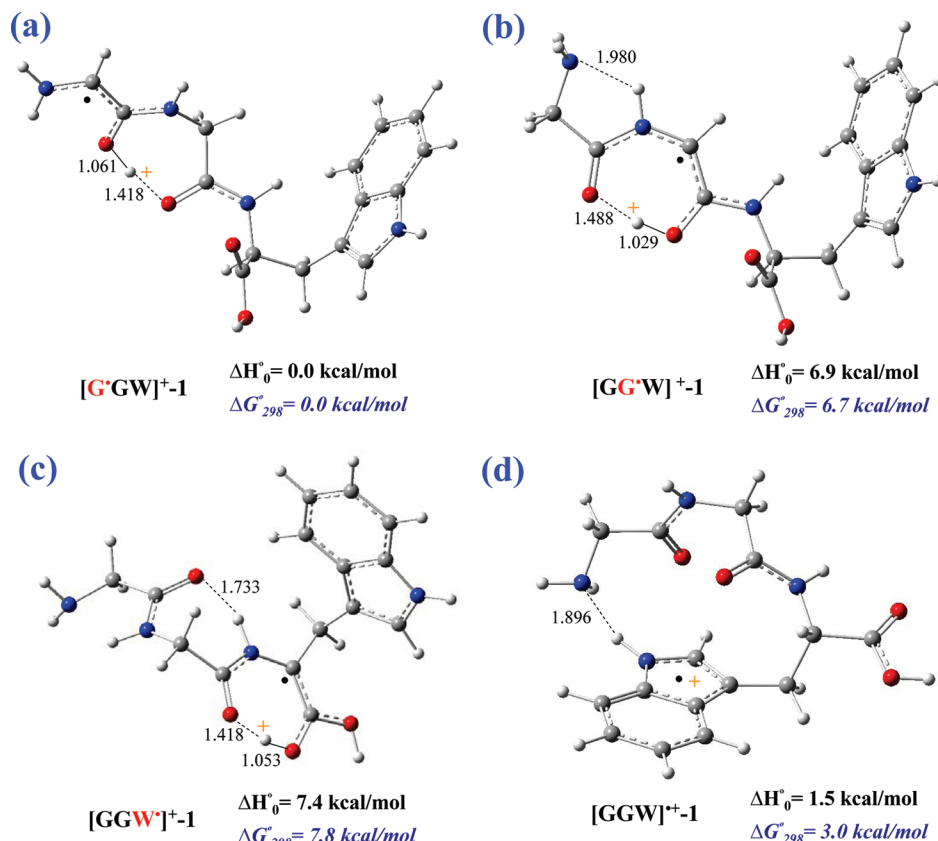


Figure 2. Optimized lowest-energy structures for $[G'GW]^{•+}$, $[GG'W]^{•+}$, $[GGW']^{•+}$, and $[GGW]^{•+}$ (bond lengths, Å). All of the line structures of Figures 2–5 are available in Figures S1–S4 of the Supporting Information.

i.e., significantly larger than that for His $^{•+}$.⁴⁰ Therefore, interconversion of the α -centered radicals to π -radical isomers may occur less readily.

Experimental Section

Materials. All chemicals were obtained commercially (Aldrich and Sigma, St Louis, MO; Bachem, King of Prussia, PA). Tripeptides, Cu(II)(terpy)(NO₃)₂ (terpy = 2,2':6',2''-terpyridine) and [Co(III)(salen)]Cl [salen = N,N'-ethylenebis(salicylidene-aminato)] complexes were synthesized according to procedures described in the literature.^{48–50}

Mass Spectrometry. All mass spectrometry experiments were conducted using a quadrupole ion trap mass spectrometer (Finnigan LCQ, ThermoFinnigan, San Jose, CA). Samples typically comprised a 600 μM metal complex and 50 μM oligopeptide in a water/MeOH (50:50) solution. A syringe pump (Cole Parmer, Vernon Hills, IL) was used (flow rate: 30 $\mu\text{L}/\text{h}$) to deliver the samples for electrospraying. CID spectra were acquired using He as the collision gas with injection and excitation times of 200 and 50 ms, respectively; the amplitude of the excitation was optimized for each experiment. The canonical radical cations $[GGW]^{•+}$, $[GAW]^{•+}$, $[GGY]^{•+}$, $[GAY]^{•+}$, $[YGW]^{•+}$, $[YAW]^{•+}$, $[WGY]^{•+}$, and $[WAY]^{•+}$ were formed through collision-induced dissociation (CID) of the complexes $[\text{Cu}^{\text{II}}(\text{terpy})(\text{M})]^{2+}$ or $[\text{Co}^{\text{III}}(\text{salen})\text{M}]^+$ ($\text{M} = \text{GGW}$, GAW, GGY, GAY, YGW, YAW, WGY, WAY). Subsequent fragmentation, through multiple stages of CID, of $[YGW]^{•+}$, $[YAW]^{•+}$, $[WGY]^{•+}$, and $[WAY]^{•+}$ resulted in cleavage of the N-terminus tyrosine side chain (as *p*-quinomethide) or the N-terminus tryptophan side chain (as 3-methylene-3*H*-indole) to yield the α -carbon-centered radical cations of $[G'GW]^{•+}$, $[G'AW]^{•+}$, $[G'GY]^{•+}$, and $[G'AY]^{•+}$, respectively.

Computational Methods. Electronic energies were calculated in the framework of DFT using the unrestricted (U) hybrid functional formulated with a mixture of Hartree–Fock exchange energy and Becke's three-parameter 1988 gradient-corrected exchange energy, and Lee–Yang–Parr (LYP) correlation energy. Atomic orbitals were described by a Gaussian-type split-valence shell 6-31++G(d,p) basis set including polarization and diffuse functions for all atoms. Low-lying structures of the molecular ions were obtained through a Monte Carlo conformational search using a semiempirical method (PM3) and Spartan software;⁵³ subsequent geometry optimizations were performed at the UB3LYP/6-31G and UB3LYP/6-31++G(d,p) levels. Additional DFT geometry optimizations for other plausible low-lying structures were also performed. The harmonic vibrational frequencies of all optimized structures were calculated to confirm that the structures were at local minima (all real frequencies) or were transition states (one imaginary frequency). The local minima associated with each transition structure were verified using the intrinsic reaction coordinate (IRC) method. Relative enthalpies at 0 K (ΔH°_0) were calculated from the electronic energies and zero-point energies (ZPVE) obtained within the harmonic approximation. Atomic charges and spin densities were evaluated using natural population analyses (NPA). All DFT calculations were conducted using the Gaussian 03 software package.⁵⁴

The microcanonical rate constant $k_i(E)$ of each unimolecular reaction i was calculated using the RRKM equation.⁵¹ The value of $k_i(E)$ is a function of the internal energy E of the reactant, relative to the energy of the structure at the global minimum on the potential energy surfaces (PES); it is given by eq 1

$$k_i(E) = \frac{\sigma W_i^{\ddagger}(E_i - E_{0i})}{h\rho_i(E_i)} \quad (1)$$

where $E_i = E - \Delta H_{0i}$ is the available vibrational energy (ΔH_{0i} is the i th reactant's enthalpy of formation at 0 K), $\rho_i(E_i)$ is the density of vibrational states of the reactant, $W_i^{\ddagger}(E_i - E_{0i})$ is the sum of the vibrational states of the transition state, E_{0i} is the corresponding critical energy for reaction, h is Planck's constant, and σ is the reaction path degeneracy, which is equal to 1 in all of the reaction pathways considered in this study. The vibrational states were directly counted using the Beyer-Swinehart algorithm.⁵²

Results and Discussion

CID Spectra of π-Centered $[\text{GGW}]^{+*}/[\text{GGY}]^{+*}$. Figure 1a and b displays CID spectra of the canonical forms of the

$[\text{GGW}]^{+*}$ and $[\text{GGY}]^{+*}$ radical cations. Fragmentation of both ions was dominated by the loss of CO_2 , resulting in the formation of dominant $[\text{a}_3 + \text{H}]^{+*}$ fragment ions and cleavage of the second N–C_α bond to produce abundant $[\text{z}_1 - \text{H}]^{+*}$ and minor $[\text{c}_2 + 2\text{H}]^{+*}$ fragments from $[\text{GGW}]^{+*}$ and solely $[\text{c}_2 + 2\text{H}]^{+*}$ from $[\text{GGY}]^{+*}$. In addition, cleavage of the N–C(O) bond produced the b_2^{+} ion from $[\text{GGY}]^{+*}$. The formation of complementary $[\text{z}_1 - \text{H}]^{+*}$ and $[\text{c}_2 + 2\text{H}]^{+*}$ ions was confirmed by examining the CID spectra of the canonical $[\text{GAW}]^{+*}$ and $[\text{GAY}]^{+*}$ precursor ions (insets to Figure 1a and b, respectively). Previous studies of canonical $[\text{GGW}]^{+*}$ radical cations have demonstrated that the radical center and the charge are formally delocalized over the aromatic ring system of the C-terminus residue.^{19,40} These processes involved the transfer of a benzylic hydrogen atom at the β -carbon atom of the C-terminal residue

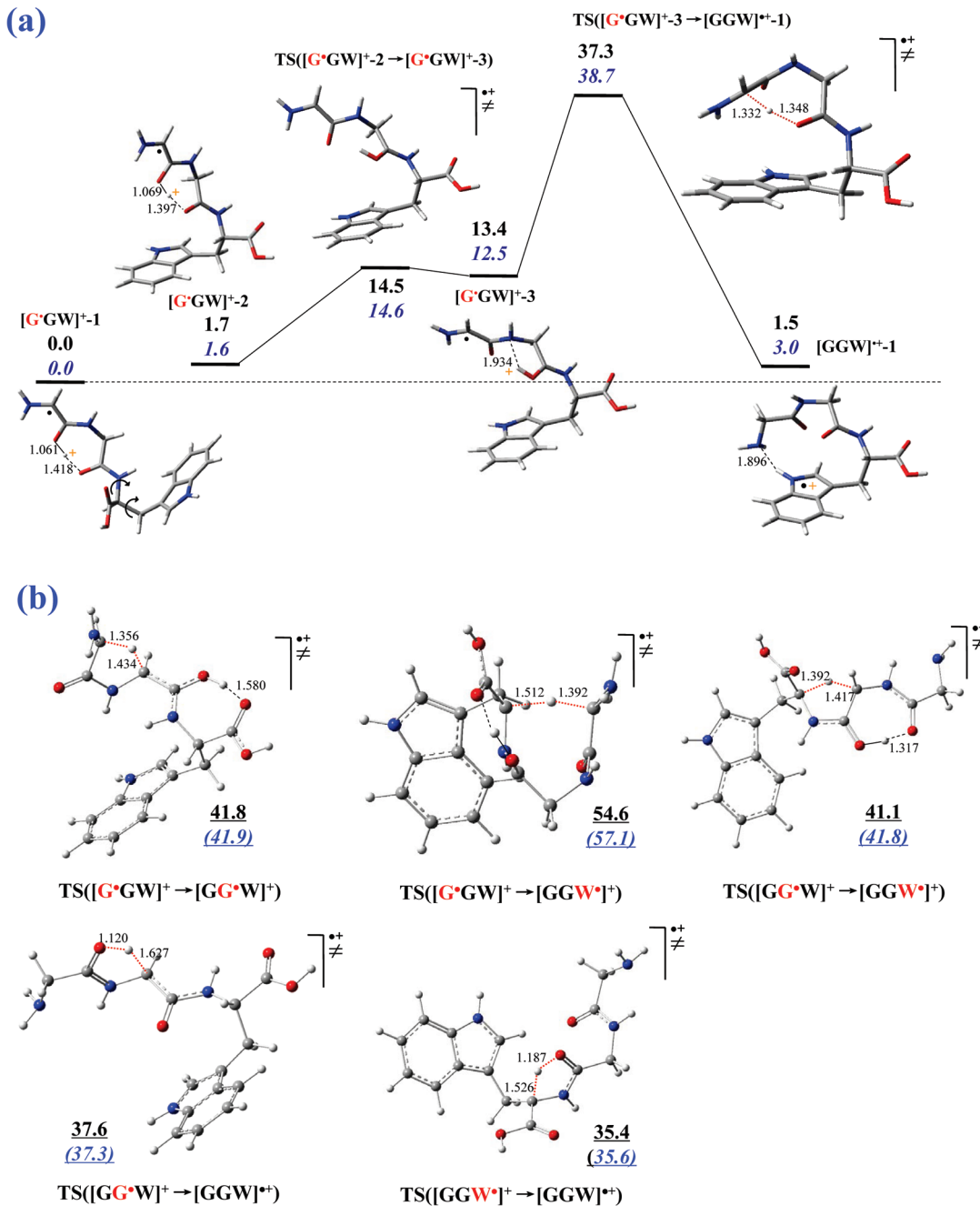


Figure 3. Isomerizations of the GGW radical cations: (a) PES for the isomerization between $[\text{G}\cdot\text{GW}]^+$ and $[\text{GGW}]^{+*}$; (b) optimized geometries of the lowest-energy transition structures for other isomerizations. The upper numbers are enthalpies at 0 K; the lower italicized numbers in parentheses are free energies at 298 K. All energies (in kcal/mol) are provided relative to $[\text{G}\cdot\text{GW}]^+\text{-1}$. Bond lengths are provided in angstroms (Å).

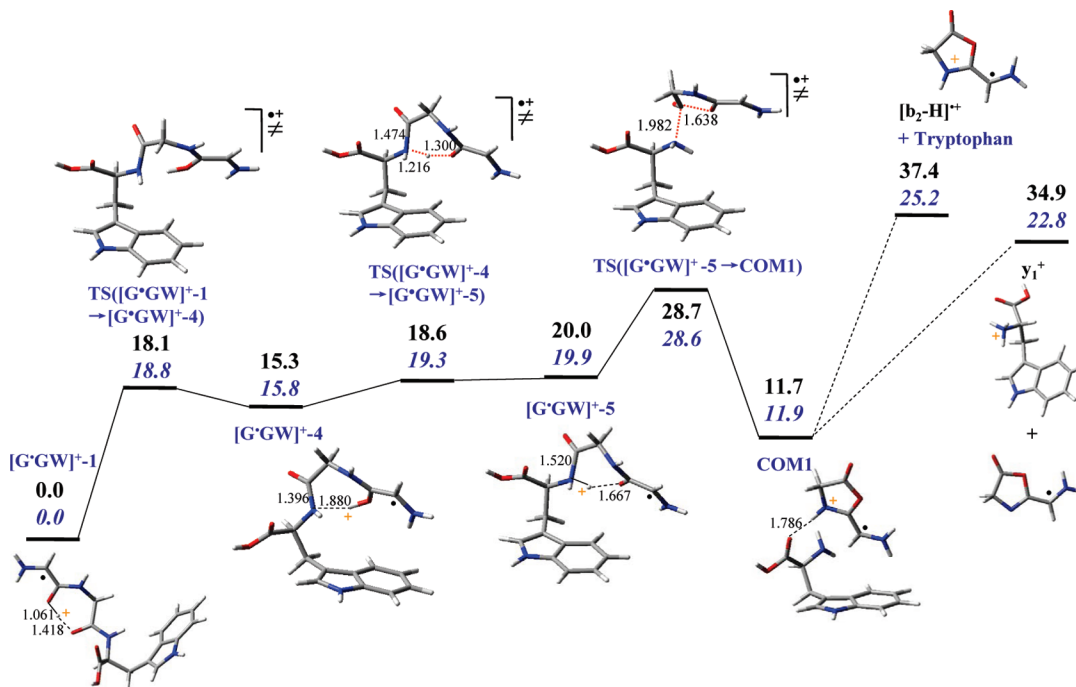


Figure 4. PES for the formation of y_1^+ and $[b_2 - H]^{2+}$ from $[G'GW]^+$. The upper numbers are enthalpies at 0 K; the lower italicized numbers in parentheses are free energies at 298 K (all energies in kcal/mol; bond lengths in Å). Solid lines connect the energy levels of minima associated with transition structures that were confirmed through IRC calculations; otherwise, the lines are broken.

to the amino group prior to $N-C_\alpha$ bond cleavage. Our results suggest that the competition between the formation of the C-terminal $[z_1 - H]^{2+}$ ion and the N-terminal $[c_2 + 2H]^{2+}$ ion is determined by the proton affinities of the tryptophanyl (PA 226.8 kcal/mol) and tyrosyl (PA 221.0 kcal/mol) residues,⁴⁶ which are in accordance with the results of $[GW]^{2+}$.⁴⁰

CID Spectra of α -Carbon-Centered $[G'GW]^+$ / $[G'GY]^+$. Radical cations with well-defined initial radical locations were produced through side chain fragmentations of the $[Y\text{GW}]^{2+}$ and $[W\text{GY}]^{2+}$ precursor radicals. Radical ions of $[Y\text{GW}]^{2+}$ and $[W\text{GY}]^{2+}$ were first generated via CID of the complexes $[\text{Cu}^{II}(L)(Y\text{GW})]^{2+}$ and $[\text{Cu}^{II}(L)(W\text{GY})]^{2+}$, respectively. Subsequent fragmentation of these radical cations resulted in formation of α -carbon-centered radicals, $[G'GW]^+$ and $[G'GY]^+$, respectively, via the losses of *p*-quinomethide and 3-methylene-3*H*-indole, respectively, from the N-terminal residues. Figure 1c and d present CID spectra of the radical cations $[G'GW]^+$ and $[G'GY]^+$ in which the initial radical sites were located on the N-terminal α -carbon atoms. We confirmed the identity of the major fragment ions by comparing the CID spectra of $[G'GW]^+$ and $[G'GY]^+$ with the spectra obtained for $[G'AW]^+$ and $[G'AY]^+$ (insets to Figure 1c and d, respectively). The fragmentations of the α -carbon-centered $[G'GW]^+$ and $[G'GY]^+$ radical cations are strikingly different from the dissociation of the corresponding canonical radicals described above. Namely, these ions dissociate mainly through the loss of water and cleavage of the second amide bond, resulting in the formation of y_1^+ and $[b_2 - H]^{2+}$ fragment ions. The distinctly different product ion spectra of the well-defined α -carbon-centered and π -aromatic radical cations of GGW suggest the presence of substantial free energy barriers for interconversion between these isomeric structures. In the following sections, we discuss the energetics and kinetics of the interconversion and fragmentation processes of GGW radical cations.

Low Energy Structures of GGW Radical Cations. Figure 2 displays the lowest-energy structures of α -carbon-centered radical cations with the radical localized at the N-terminal,

middle, and C-terminal residues ($[G'GW]^+ \mathbf{-1}$, $[GG'W]^+ \mathbf{-1}$, and $[GG'W]^+ \mathbf{-1}$, respectively) and the π -radical cation in which the radical is delocalized on the indolyl ring of the tryptophan residue ($[GGW]^+ \mathbf{-1}$). As with the GGG radical cation,^{43,44} the global minimum on the PES of the GGW radical cation is $[G'GW]^+ \mathbf{-1}$, in which the radical and proton are located on the N-terminal α -carbon and amide oxygen atoms, respectively, forming a captodatively stabilized structure. In $[GG'W]^+ \mathbf{-1}$, a relatively weak electron donating group ($-\text{CONH}$) and a strong electron withdrawing group ($(-\text{C(OH)}\text{NH})^+$) surround the radical center. A seven-membered ring containing a short (1.488 Å) $[\text{CO}_1 \cdots \text{H}-\text{O}_2\text{C}]$ hydrogen bond (the italicized subscripts refer to the residue number counting from the N-terminus) delocalizes some of the positive charge between the N-terminal amide group and the C-terminal amide group. The combined effects of both the weaker electron donating group and the hydrogen bond delocalization in $[GG'W]^+ \mathbf{-1}$ reduce the captodative stabilization, making $[GG'W]^+ \mathbf{-1}$ higher enthalpy than $[G'GW]^+ \mathbf{-1}$ by 6.9 kcal/mol.

Previous comparisons^{19,43} between spin and charge distributions and the relative energies of $[G'GW]^+ \mathbf{-1}/[GG'W]^+ \mathbf{-1}$ and $[G'GG]^+ \mathbf{-1}/[GG'G]^+ \mathbf{-1}$ radical cations have revealed that the presence of a tryptophan residue in the sequence has very little influence on the structures and relative stabilities of the two α -carbon-centered radical cations. Because the aromatic residue is present, however, both the charge and spin density distribution and the relative stability of the canonical $[GG'W]^+ \mathbf{-1}$ and $[GGG]^+ \mathbf{-1}$ radical cations are substantially different. Natural population analysis of $[GGW]^+ \mathbf{-1}$ revealed that the radical and charge are delocalized mainly on the tryptophan side chain, which greatly contributes to the stability of this canonical radical cationic form; $[GGW]^+ \mathbf{-1}$ is only 1.5 kcal/mol higher in enthalpy than the lowest-energy captodative structure, $[G'GW]^+ \mathbf{-1}$. In contrast, the lowest-energy structure of the canonical GGG radical cation has its highest charge and spin on the amino group; it is higher in enthalpy than its lowest-energy captodative structure, $[G'GG]^+ \mathbf{-1}$, by 30.3 kcal/mol. Similar charge

TABLE 1: Proton Affinities (ΔH_{298}°)^a of Fragments Resulting from Amide Bond and N–C_α Bond Cleavage

[b₂ - H]^{•+} vs. y₁⁺			
N-terminal fragment	PA (kcal/mol)	C-terminal fragment	PA (kcal/mol)
	224.3 (R ₁ = H)	Tryptophan	227.4 (226.8 ^b)
	227.0 (R ₁ = CH ₃)	Tyrosine	224.0 (221.0 ^b)
[c₂+2H]⁺ vs. [z₁ - H]^{•+}			
	225.5 (R ₁ =H; 225.7 ⁴⁰)	Indolyl radical	228.0 (227.6 ⁴⁰)
	226.8 (R ₁ = CH ₃)	Phenoxy radical	213.2 (212.7 ⁴⁰)

^a All PAs calculated at the B3LYP/6-31++G(d,p) level. ^b From NIST Chemistry WebBook: <http://webbook.nist.gov/chemistry/>.

and spin distributions are found for the tryptophan radical cations **Trp1** and **Trp2** and the corresponding GGW radical cations **[GGW]^{•+1}** and **[G'GW]^{•+1}**, respectively. The relative energies of **Trp1** vs **Trp2**²⁰ and **[GGW]^{•+1}** vs **[G'GW]^{•+1}** are 1.0 and –1.4 kcal/mol, respectively.

In **[GGW]^{•+1}**, the proton detached from the α-carbon atom of the third residue is located on the carboxylic oxygen atom and is hydrogen bonded to the carbonyl oxygen atom of the C-terminal peptide bond ([CO₃–H⁺⋯⋯O₂C] hydrogen bond length: 1.418 Å). This α-carbon-centered radical cation is stabilized by the captodative effect and also by the presence of the tryptophan side chain, forming a tertiary carbon radical center. In addition, the N-terminal amide oxygen atom donates some electron density to the C-terminal amide bond via a strong [N₃H⋯⋯O₁C] hydrogen bond (1.733 Å), which further enhances the captodative effect. Together, all of these factors result in **[GGW]^{•+1}** being only 7.4 kcal/mol higher in enthalpy than **[G'GW]^{•+1}** and almost isoenergetic with **[GG'W]^{•+1}**.

Interconversion between GGW Radical Cations. Figure 3a displays the potential energy surface for the interconversion between **[G'GW]^{•+1}** and **[GGW]^{•+1}**. From **[G'GW]^{•+1}**, rotations (data not shown) about the C_α–C_β and N–C_α bonds of the third residue give **[G'GW]^{•+2}**, which is only 1.7 kcal/mol higher in enthalpy than **[G'GW]^{•+1}**. Proton transfer from CO₁ to O₂C and rotation of the C–C_α bond of the second residue

break the strong hydrogen bond [CO₁H⁺⋯⋯O₂C] in the seven-membered ring of **[G'GW]^{•+2}**, resulting in a much weaker [CO₂H⁺⋯⋯N₂H] hydrogen bond (1.934 Å) in **[G'GW]^{•+3}**. The energy barrier of this step is 14.5 kcal/mol higher than the energy of **[G'GW]^{•+1}**. The following step of this reaction is rate-determining: a 1,6-hydrogen atom transfer from the carbonyl oxygen atom of the second residue to the α-carbon atom of the first residue has a reaction barrier of 37.3 kcal/mol. After overcoming this energy barrier, the lowest-energy isomer of **[GGW]^{•+1}** is formed with a substantial reverse energy barrier (35.8 kcal/mol). The forward barrier of this reaction is comparable to that for interconversion from **[G'GG]⁺** to **[GGG]⁺** (39.5 kcal/mol),⁴³ indicating that the presence of the tryptophan side chain barely affects this process. The reverse interconversion from **[GGW]^{•+1}** to **[G'GW]^{•+1}** is, however, associated with a fairly high barrier of 35.8 kcal/mol, relative to the 9.2 kcal/mol required for interconversion from **[GGG]⁺** to **[G'GG]⁺**.⁴⁴

Figure 3b presents the lowest-energy transition structures (TSs) for other isomerizations among the GGW radical cations with different radical sites. The energy barrier for interconversion between **[G'GW]⁺** and **[GG'W]⁺** (41.8 kcal/mol) is ca. 3 kcal/mol lower than that between **[G'GG]⁺** and **[GG'G]⁺** (44.7 kcal/mol). The interconversion barriers among the GGW radical cations are slightly lower than those among the GGG radical

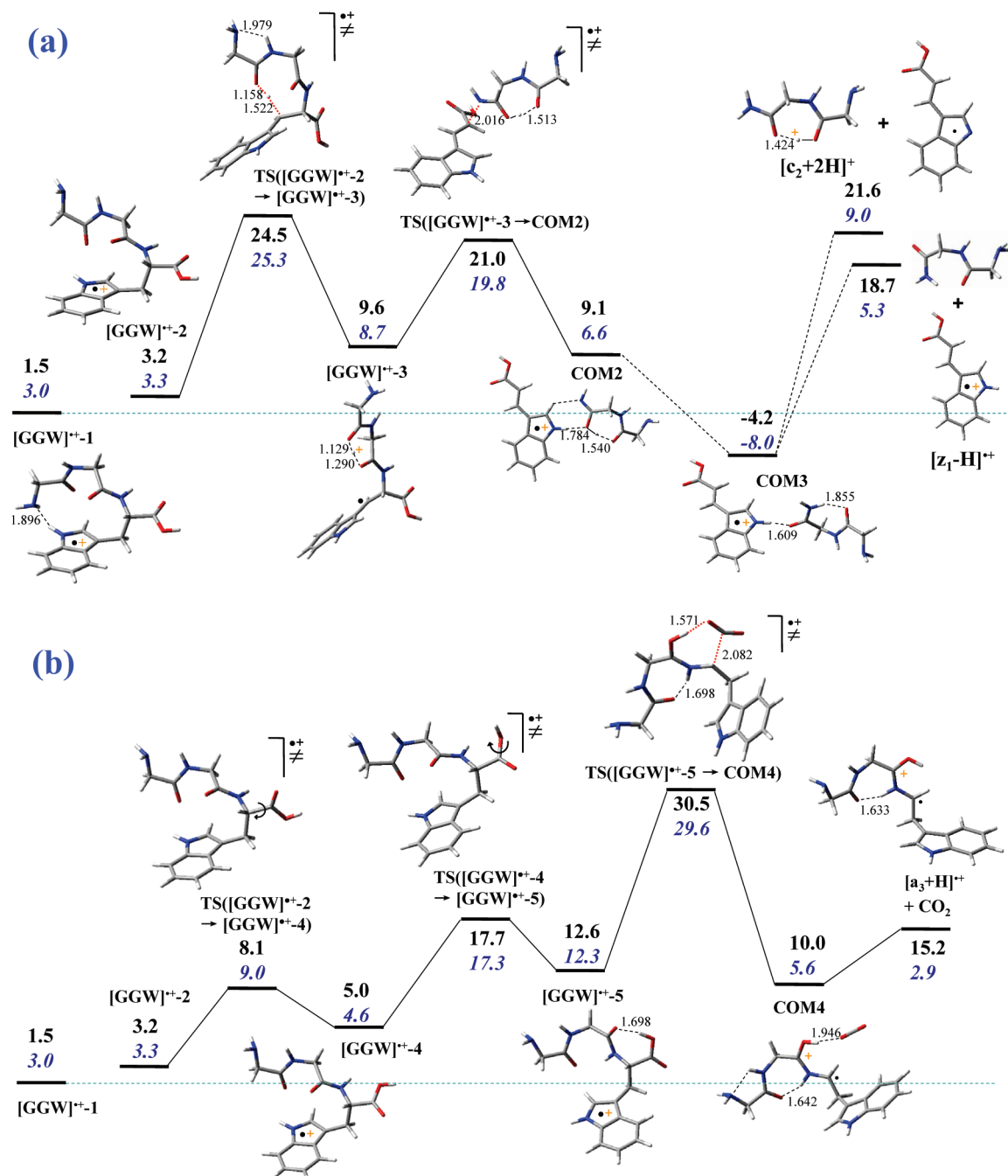


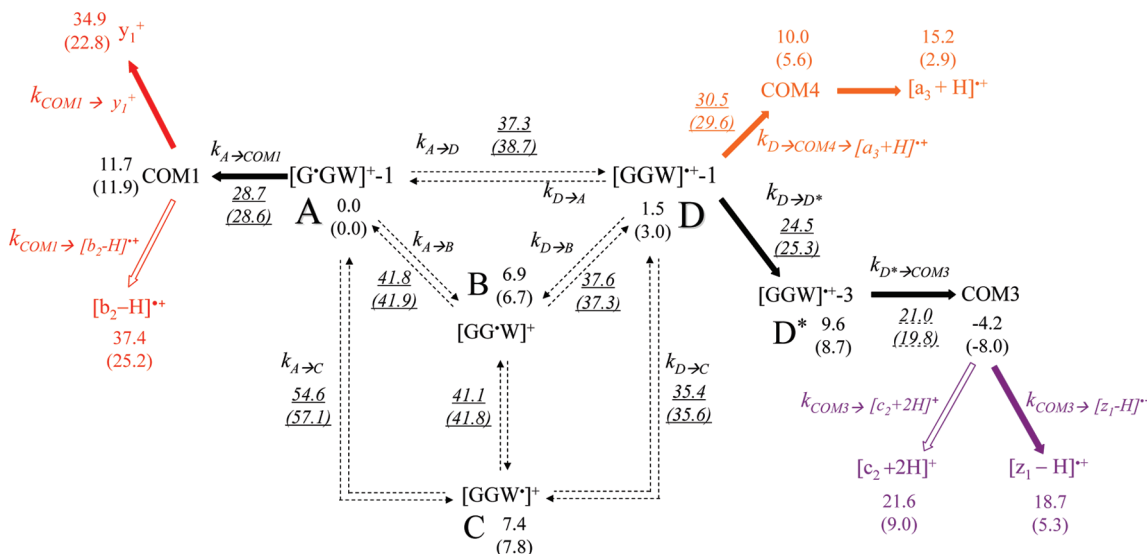
Figure 5. PES for the formation of (a) $[c_2 + 2H]^+$ and $[z_1 - H]^+$ and (b) $[a_3 + H]^+ + CO_2$ from $[GGW]^+$. The upper numbers are enthalpies at 0 K; the lower italicized numbers are free energies at 298 K (all energies in kcal/mol; bond lengths in Å). Solid lines connect energy levels of the minima associated with each transition structure that were confirmed through IRC calculations; otherwise, the lines are broken.

cations by ca. 8 kcal/mol,⁴³ presumably because of the stabilizing effect of the tertiary carbon radical center from tryptophan.

Potential Energy Surfaces for the Fragmentations of $[G'GW]^+$ and $[GGW]^+$. *I. $[G'GW]^+$.* Figure 4 displays the potential energy surface for formation of the y_1^+ and $[b_2 - H]^+$ ions from $[G'GW]^{+-1}$. Rotation of $[G'GW]^{+-1}$ about the $C_\alpha - C$ bond of the second glycine residue destroys the strong $[CO_1H^+ \cdots O_2C]$ hydrogen bond (1.418 Å) in the seven-membered ring and forms a much weaker $[CO_1 - H^+ \cdots N_3H]$ hydrogen bond (1.880 Å) in a shallow local minimum, $[G'GW]^{+-4}$, which is 15.3 kcal/mol higher in enthalpy than $[G'GW]^{+-1}$. After undergoing a 1,6-proton transfer process having a forward energy barrier of only 3.3 kcal/mol, an unstable intermediate $[G'GW]^{+-5}$ is formed in which the proton is attached to the

nitrogen atom of the C-terminal amide bond, which greatly weakens the C-terminal amide bond (its bond length increases from 1.396 Å in $[G'GW]^{+-4}$ to 1.520 Å in $[G'GW]^{+-5}$). Nucleophilic attack by the N-terminal amide oxygen atom on the C-terminal amide carbon atom cleaves the C-terminal amide bond and forms a proton-bound dimer, **COM1**, between neutral tryptophan and the $[b_2 - H]^+$ radical cation.

The energy barriers for the formation of the y_1^+ and $[b_2 - H]^+$ species from $[G'GW]^{+-1}$ are 34.9 and 37.4 kcal/mol, respectively; these values are comparable with the interconversion barrier between $[G'GW]^{+-1}$ and $[GGW]^{+-1}$ (37.3 kcal/mol), indicating that some of the $[G'GW]^+$ species could interconvert to $[GGW]^+$ during CID. Isomerization of a small fraction of $[G'GW]^+$ ions into $[GGW]^+$ prior to fragmentation

SCHEME 1: Isomerizations and Dissociations of GGW Radical Cations^a

^a Relative enthalpies ΔH° and relative free energies ΔG°_{298} (in parentheses) were evaluated (in kcal/mol) at the UB3LYP/6-31++G(d,p) level. The underlined values are critical energy barriers. The isomerizations between the α-carbon-centered radical cations are indicated by dashed arrows. The RRKM rate constants for the key competitive isomerizations and fragmentations of $[G^*GW]^+$ and $[GGW]^+$ radical cations are placed on the arrows.

is responsible for the formation of a minor $[z_1 - H]^{•+}$ fragment—the most abundant CID product of $[GGW]^+$ (Figure 1a)—from the $[G^*GW]^+$ precursor ion (Figure 1c).

The competition between the formation of y_1^+ and $[b_2 - H]^{•+}$ species from $[G^*GX]^+$ and $[G^*AX]^+$ ($X = Y$ or W) correlates with the relative proton affinities (PAs) of the two possible neutral fragments (see Table 1), suggesting that dissociation of the proton-bound dimer is the last step of this decomposition pathway. Formation of the dominant y_1^+ ion from $[G^*GW]^+$ and $[G^*AW]^+$ is favored because the PA of tryptophan (227.4 kcal/mol) is greater than the PAs of the N-terminal oxazolone (224.3 kcal/mol) and methyl-oxazolone (227.0 kcal/mol) fragments. In contrast, dissociation of $[G^*GY]^+$ produced a heterodimer, comprising a deprotonated oxazolone and tyrosine, which have almost identical PAs. This result is consistent with the almost equal abundance of y_1^+ and $[b_2 - H]^{•+}$ fragment ions observed in the spectrum of $[G^*GY]^+$. In contrast, the formation of the y_1^+ ion from $[G^*AY]^+$ is suppressed because the PA of methyl-oxazolone (227.0 kcal/mol) is higher than that of tyrosine (224.0 kcal/mol), favoring the formation of the $[b_2 - H]^{•+}$ ion.

II. $[GGW]^+$. Figure 5a displays the potential energy surface for the formation of $[z_1 - H]^{•+}$ and $[c_2 + 2H]^{•+}$ species from $[GGW]^+ - 1$, which are in accordance with the results of $[GW]^+.$ ⁴⁰ Rotation about the $C_\alpha - C$ bond of the first glycine residue in $[GGW]^+ - 1$ gives $[GGW]^+ - 2$ (transition state not shown), which is only 1.7 kcal/mol higher in enthalpy than $[GGW]^+ - 1$. Proton transfer from the β-carbon atom of tryptophan to the carbonyl oxygen atom of the first residue gives the distonic ion $[GGW]^+ - 3$, which has a relative energy of 9.6 kcal/mol; here, the radical delocalized on the indole π-system. In addition, $[GGW]^+ - 3$ is stabilized by a seven-membered ring containing a very strong $[CO_1H^+ \cdots O_2C]$ hydrogen bond (1.290 Å). This proton transfer is the rate-determining step (energy barrier: 24.5 kcal/mol). Subsequent heterolytic cleavage of the $N_3 - C_\alpha$ bond, with both the charge and radical remaining on the C-terminal fragment, results in a proton-bound dimer (**COM2**) of the $[z_1 - H]^{•+}$ ion and the iminol tautomer of glycylglycinamide connected by hydrogen bonds. The energy

barrier against this step is 21.0 kcal/mol. Rotations of the large groups within the ion-neutral complexes are associated with low barriers to form the low-energy complexes **COM3** (−4.2 kcal/mol). Direct dissociation of **COM3** gives a tautomer of $[z_1 - H]^{•+}$ and glycylglycinamide, while proton transfer from the nitrogen atom of the indole ring to the glycylglycinamide oxygen atom, followed by dissociation, gives the $[c_2 + 2H]^{•+}$ ion and protonated glycylglycinamide. The relative energy of the formation of $[z_1 - H]^{•+}$ is 2.9 kcal/mol lower than that of $[c_2 + 2H]^{•+}$, because of the different PAs of the two incipient fragments in the proton-bound dimer, consistent with the experimental results. Again, the branching ratio of $[z_1 - H]^{•+}/[c_2 + 2H]^{•+}$ in Figure 1a and b for other tripeptide radical cations can be explained by considering the PAs of the various fragments in Table 1.⁴⁰

Figure 5b displays the potential energy surface for the formation of $[a_3 + H]^{•+}$ and CO_2 . Rotation of the carboxylic group of $[GGW]^+ - 2$ destroys the weak $[N_3H \cdots O_3C]$ hydrogen bond (2.248 Å) and forms a weaker $[N_3H \cdots O_3H]$ hydrogen bond (2.281 Å) in $[GGW]^+ - 4$, followed by rotation about the $C - OH$ bond to form the critical intermediate $[GGW]^+ - 5$, which is 11.1 kcal/mol higher in enthalpy than $[GGW]^+ - 1$ and features a strong $[O_3H \cdots O_2C]$ hydrogen bond (1.698 Å). Hydrogen atom transfer from the hydroxyl group to the carbonyl oxygen atom facilitates the cleavage of the $C_\alpha - C$ bond to form a tautomer of the $[a_3 + H]^{•+}$ ion by eliminating CO_2 via **COM4**; the rate-determining step of this reaction possesses a moderate energy barrier of 30.5 kcal/mol. The charge and spin of $[a_3 + H]^{•+}$ are delocalized on the C-terminal protonated amide bond and the α-carbon atom, respectively. Scheme 1 summarizes the isomerizations and dissociations of the GGW radical cations. Because the isomerization barriers for GGW radical cations are only slightly higher than the competing fragmentation barriers, it is difficult to determine the extent of isomerization prior to dissociation of the GGW radical cations based on the calculated barrier heights alone. In the following section, we describe the results of RRKM calculations of reaction rate constants that provide further insight on the competition between isomerization and fragmentation.

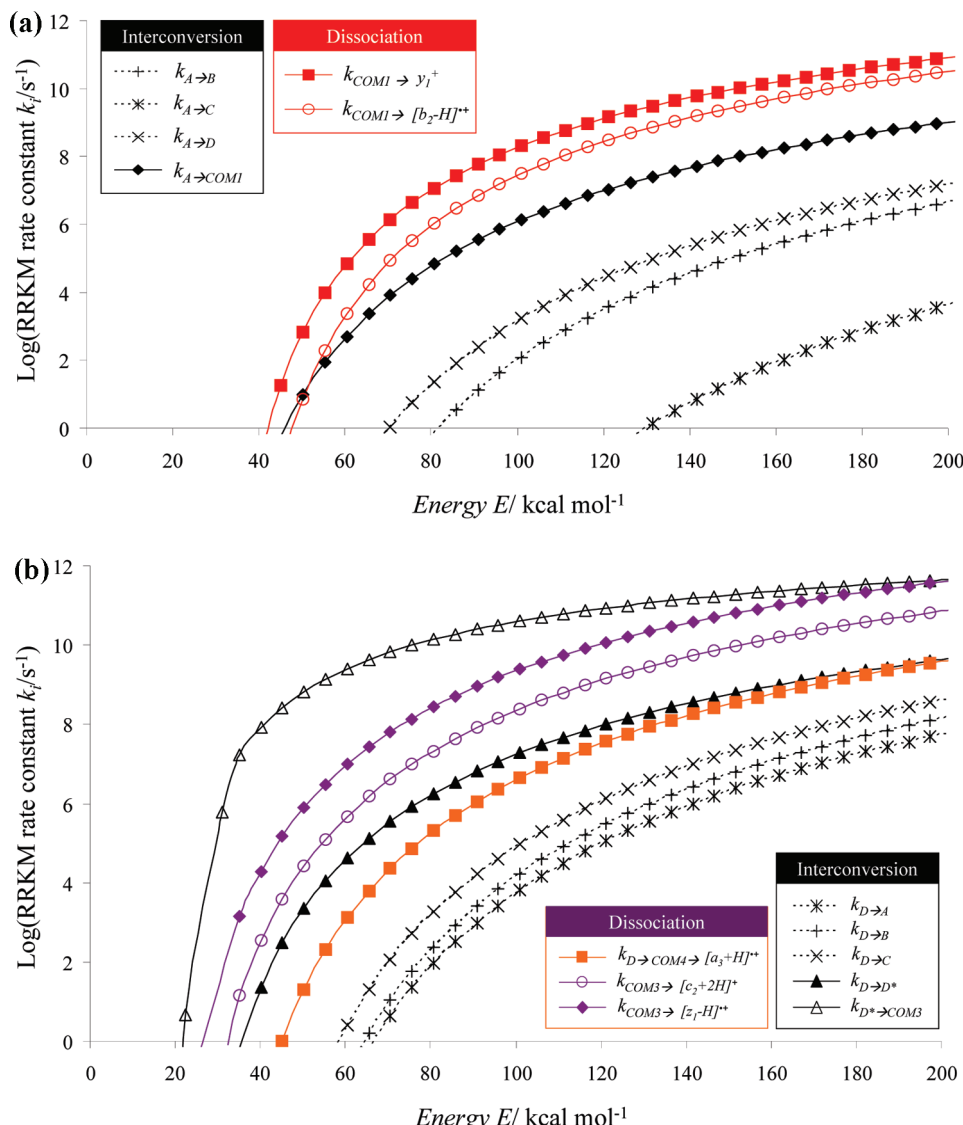


Figure 6. RRKM modeling for the key competitive isomerizations and fragmentations of (a) $[G'GW]^{+}$ and (b) $[GGW]^{+}$ radical cations; RRKM rate constants, $\log k_i$ (s^{-1}), plotted with respect to internal energies E (kcal/mol).

TABLE 2: Relative Energies at 0 K (ΔH_0° , kcal/mol) of Tautomers of the GGW Radical Cations, Their Dissociation Products, and Activation Barriers at 0 K (E_0 , kcal/mol) and Entropies at 298 K (ΔS_{298}^\ddagger ,^a cal/mol·K)^b

relative energies of tautomers				relative energies of products				
ΔH_0°				ΔH_0°				
$[G'GW]^{+}$ -1 (A)	0.0			$[b_2 - H]^{+}$ + Trp			37.4	
$[GG'W]^{+}$ -1 (B)	6.9			y_1^{+} + $[b_2 - 2H]^{+}$			34.9	
$[GGW]^{+}$ -1 (C)	7.4			$[c_2 + 2H]^{+}$ + $[z_1 - 2H]^{+}$			21.6	
$[GGW]^{+}$ -1 (D)	1.5			$[z_1 - H]^{+}$ + glycylglycinamide			18.7	
$[GGW]^{+}$ -3 (D*)	9.6							
dissociation barriers								
	ΔH_0° ^c	ΔH_0° ^d	E_0 ^e	ΔS_{298}^\ddagger	ΔH_0° ^c	ΔH_0° ^d	E_0 ^e	ΔS_{298}^\ddagger
COM1 → $[b_2 - H]^{+}$	11.7	37.4	25.7	6.1	A → B	0.0	41.8	-1.3
COM1 → y_1^{+}	11.7	34.9	23.2	4.8	A → C	54.6	54.6	-4.4
COM3 → $[c_2 + 2H]^{+}$	5.6	21.6	16.0	7.3	A → D	37.3	37.3	-2.3
COM3 → $[z_1 - H]^{+}$	-4.2	18.7	22.9	8.2	D → A	1.5	37.3	-1.2
					D → B	37.6	36.1	1.6
						D → COM4	1.5	30.5
							29.0	2.1

^a Please refer to Table S1 in the Supporting Information for the details regarding the calculation of ΔS_{298}^\ddagger . ^b All energies are relative to the lowest-energy tautomer $[G'GW]^{+}$ -1 (A) and were calculated at the UB3LYP/6-31++G(d,p) level. ^c ΔH_0° (relative energies of reactants). ^d ΔH_0° (relative energies of transition states or products). ^e $E_0 = {}^3\Delta H_0^\circ - 2\Delta H_0^\circ$.

RRKM Modeling of GGW Radical Cations. Scheme 1 summarizes the isomerization and fragmentation reactions of

GGW radical cations. Each potential energy surface was simplified by only keeping the critical steps for RRKM

calculations. Microcanonical rate constants were calculated for all possible decay channels of $[G^{\bullet}GW]^+$ and $[GGW]^{+\bullet}$ using relative energies and vibrational frequencies obtained from DFT calculations. Figure 6 displays the calculated values of $k_i(E)$ for the $[G^{\bullet}GW]^+$ and $[GGW]^{+\bullet}$ precursor ions. Clearly, the isomerization rates are much slower than the fragmentation rates for both precursor ions. For example, the rate constants for isomerization of $[G^{\bullet}GW]^{+\bullet}\text{-1 (A)}$ into $[GGW]^{+\bullet}\text{-1 (B)}$ or $[GGW]^{+\bullet}\text{-1 (D)}$ are 3–4 orders of magnitude lower than that for isomerization into **COM1**, a critical intermediate that subsequently yields $[b_2 - H]^{+\bullet}$ and $y_1^{+\bullet}$ reaction products. Formation of the **COM1** intermediate is a rate-determining step for the formation of these fragment ions at all internal excitation energies, except at very low internal excitation energy, where fragmentation of **COM1** becomes slower than isomerization into **COM1**. Similarly, isomerization of the $[GGW]^{+\bullet}\text{-1 (D)}$ ion into the reactive intermediate $[GGW]^{+\bullet}\text{-3 (D*)}$ (black line with filled triangle markers in Figure 6b)—a rate-determining step for the formation of $[c_2 + 2H]^{+\bullet}$ and $[z_1 - H]^{+\bullet}$ fragment ions—is much faster than isomerization of $[GGW]^{+\bullet}\text{-1 (D)}$ into $[G^{\bullet}GW]^{+\bullet}\text{-1 (A)}$ and $[GGW]^{+\bullet}\text{-1 (B)}$, while the rate-limiting step for fragmentation of the π-radical forming $[a_3 + H]^{+\bullet}$ ion (orange line with filled square markers in Figure 6b) is at least 2 orders of magnitude faster than isomerization into other α-radical isomers. These results further confirm that the fragmentation pathways of $[G^{\bullet}GW]^+$ and $[GGW]^{+\bullet}$ ions are much faster than isomerization between these two structures. Table 2 lists the activation entropies for the interconversions and fragmentation reactions. We obtained similar entropy effects (0–2 cal/mol/K) for all isomerization reactions; the fragmentation steps are, however, characterized by substantially more positive activation entropies, characteristic of reactions lacking reverse activation barriers.

Conclusion

We have experimentally generated two nonconvertible isomeric radical cationic tripeptides of glycylglycyltryptophan— $[G^{\bullet}GW]^+$ and $[GGW]^{+\bullet}$ —with well-defined initial radical sites at the α-carbon atom and the 3-methylindole ring, respectively. Low energy CID of $[GGW]^{+\bullet}$ produced fragment ions of the types $[a_3 + H]^{+\bullet}$ and $[z_1 - H]^{+\bullet}$; in contrast, $[G^{\bullet}GW]^+$ formed the $y_1^{+\bullet}$ ion predominantly. We used DFT calculations and RRKM modeling to examine the competition between the isomerization and dissociation processes of the isomers. The distinct differences in their dissociation products can be understood in terms of the relatively high barriers for interconversion relative to those of the competing dissociation pathways. RRKM calculations confirmed that the relatively high rate constants for the dissociation reactions of both the $[G^{\bullet}GW]^+$ and $[GGW]^{+\bullet}$ radical cations hindered their isomerizations.

Acknowledgment. Most of the research described in this manuscript was supported by the University of Hong Kong (UGC) and the Hong Kong Research Grants Council, Special Administrative Region, China (Project No. HKU 7018/06P and Project No. HKU 7012/08P). D.C.M.N. and T.S. thank the Hong Kong RGC for supporting their studentship. J.L. acknowledges support from the Chemical Sciences Division, Office of Basic Energy Sciences of the U. S. Department of Energy. Part of the work presented here was performed at the W. R. Wiley Environmental Molecular Sciences Laboratory (EMSL), a national scientific user facility sponsored by the U.S. Department of Energy's Office of Biological and Environmental Research and located at Pacific Northwest National Laboratory (PNNL).

PNNL is operated by Battelle for the U.S. Department of Energy. C.K.S. is grateful for financial support from the City University of Hong Kong.

Supporting Information Available: Table showing relative energies of tautomers of the GGW radical cations, activation barriers of interconversion, and entropies obtained from the Gaussian 03 output files, figures showing optimized lowest-energy structures for the GGW radical cations, isomerizations of the GGW radical cations, and potential energy surfaces, and a list of the total energies and Cartesian coordinates predicted for the stationary points in Figures 2–5 with the B3LYP/6-31++G(d,p) method. This material is available free of charge via the Internet at <http://pubs.acs.org>.

References and Notes

- (1) Opazo, C.; Huang, X.; Cherny, R. A.; Moir, R. D.; Roher, A. E.; White, A. R.; Cappai, R.; Masters, C. L.; Tanzi, R. E.; Inestrosa, N. C.; Bush, A. I. *J. Biol. Chem.* **2002**, *277*, 40302.
- (2) Millhauser, G. L. *Acc. Chem. Res.* **2004**, *37*, 79.
- (3) Hawkins, C. L.; Davies, M. J. *Biochim. Biophys. Acta, Bioenerg.* **2001**, *1504*, 196.
- (4) Holm, R. H.; Kennepohl, P.; Solomon, E. I. *Chem. Rev.* **1996**, *96*, 2239.
- (5) Stubbe, J.; van der Donk, W. A. *Chem. Rev.* **1998**, *98*, 705.
- (6) Zubarev, R. A.; Horn, D. M.; Fridriksson, E. K.; Kelleher, N. L.; Kruger, N. A.; Lewis, M. A.; Carpenter, B. K.; McLafferty, F. W. *Anal. Chem.* **2000**, *72*, 563.
- (7) Zubarev, R. A. *Curr. Opin. Biotechnol.* **2004**, *15*, 12.
- (8) Syka, J. E. P.; Coon, J. J.; Schroeder, M. J.; Shabanowitz, J.; Hunt, D. F. *Proc. Natl. Acad. Sci. U.S.A.* **2004**, *101*, 9528.
- (9) Han, H. L.; Xia, Y.; McLuckey, S. A. *J. Proteome Res.* **2007**, *6*, 3062.
- (10) (a) Hopkinson, A. C. ; Siu, K. W. M. In *Principles of Mass Spectrometry Applied to Biomolecules*; Laskin, J., Lifshitz, C., Eds.; John Wiley and Sons: New York, 2006, p 301. (b) Hopkinson, A. C. *Mass Spectrom. Rev.* **2009**, *28*, 655. (c) Ly, T.; Julian, R. R. *Angew. Chem., Int. Ed.*, in press.
- (11) Barlow, C. K.; McFadyen, W. D.; O'Hair, R. A. J. *J. Am. Chem. Soc.* **2005**, *127*, 6109.
- (12) Laskin, J.; Yang, Z. B.; Lam, C.; Chu, I. K. *Anal. Chem.* **2007**, *79*, 6607.
- (13) Hvelplund, P.; Nielsen, S. B.; Sorensen, M.; Andersen, J. U.; Jorgensen, T. J. D. *J. Am. Soc. Mass Spectrom.* **2001**, *12*, 889.
- (14) Levis, R. J. *Annu. Rev. Phys. Chem.* **1994**, *45*, 483.
- (15) Hodyss, R.; Cox, H. A.; Beauchamp, J. L. *J. Am. Chem. Soc.* **2005**, *127*, 12436.
- (16) Matsumoto, Y.; Watanabe, K. *Chem. Rev.* **2006**, *106*, 4234.
- (17) Ly, T.; Julian, R. R. *J. Am. Chem. Soc.* **2008**, *130*, 351.
- (18) Zhang, L.; Reilly, J. P. *J. Am. Soc. Mass Spectrom.* **2009**, *20*, 1378.
- (19) Bagheri-Majdi, E.; Ke, Y. Y.; Orlova, G.; Chu, I. K.; Hopkinson, A. C.; Siu, K. W. M. *J. Phys. Chem. B* **2004**, *108*, 11170.
- (20) (a) Siu, C. K.; Ke, Y.; Guo, Y.; Hopkinson, A. C.; Siu, K. W. M. *Phys. Chem. Chem. Phys.* **2008**, *10*, 5908. (b) Steill, J.; Zhao, J.; Siu, C. K.; Ke, Y.; Verkerk, U. H.; Oomens, J.; Dunbar, R. C.; Hopkinson, A. C.; Siu, K. W. M. *Angew. Chem., Int. Ed.* **2008**, *47*, 9666.
- (21) (a) Chu, I. K.; Rodriguez, C. F.; Lau, T. C.; Hopkinson, A. C.; Siu, K. W. M. *J. Phys. Chem. B* **2000**, *104*, 3393. (b) Wee, S.; O'Hair, R. A. J.; McFadyen, W. D. *Rapid Commun. Mass Spectrom.* **2002**, *16*, 884.
- (22) Wee, S.; O'Hair, R. A. J.; McFadyen, W. D. *Int. J. Mass Spectrom.* **2004**, *234*, 101.
- (23) Laskin, J.; Futrell, J. H.; Chu, I. K. *J. Am. Chem. Soc.* **2007**, *129*, 9598.
- (24) Ryzhov, V.; Lam, A. K. Y.; O'Hair, R. A. J. *J. Am. Soc. Mass Spectrom.* **2009**, *20*, 985.
- (25) O'Connor, P. B.; Lin, C.; Cournoyer, J. J.; Pittman, J. L.; Belyayev, M.; Budnik, B. A. *J. Am. Soc. Mass Spectrom.* **2006**, *17*, 576.
- (26) Leymarie, N.; Costello, C. E.; O'Connor, P. B. *J. Am. Chem. Soc.* **2003**, *125*, 8949.
- (27) Tureček, F.; Carpenter, F. H. *J. Chem. Soc., Perkin Trans. 2* **1999**, *2315*.
- (28) Tureček, F.; Jones, J. W.; Towle, T.; Panja, S.; Brøndsted Nielsen, S.; Hvelplund, P.; Paizs, B. *J. Am. Chem. Soc.* **2008**, *130*, 14584.
- (29) Tureček, F.; Carpenter, F. H.; Polce, M. J.; Wesdemiotis, C. *J. Am. Chem. Soc.* **1999**, *121*, 7955.

- (30) Hayakawa, S.; Matsubara, H.; Panja, S.; Hvelplund, P.; Brøndsted Nielsen, S.; Chen, X.; Tureček, F. *J. Am. Chem. Soc.* **2008**, *130*, 7645.
- (31) Polce, M. J.; Wesdemiotis, C. *J. Mass Spectrom.* **2000**, *35*, 251.
- (32) Simon, S.; Sodupe, M.; Bertran, J. *J. Phys. Chem. A* **2002**, *106*, 5697.
- (33) Simon, S.; Gil, A.; Sodupe, M.; Bertran, J. *THEOCHEM* **2005**, *727*, 191.
- (34) Gil, A.; Simon, S.; Sodupe, M.; Bertran, J. *Chem. Phys. Lett.* **2008**, *451*, 276.
- (35) Moran, D.; Jacob, R.; Wood, G. P. F.; Coote, M. L.; Davies, M. J.; O'Hair, R. A. J.; Easton, C. J.; Radom, L. *Helv. Chim. Acta* **2006**, *89*, 2254.
- (36) Menon, A. S.; Wood, G. P. F.; Moran, D.; Radom, L. *J. Phys. Chem. A* **2007**, *111*, 13638.
- (37) Wood, G. P. F.; Gordon, M. S.; Radom, L.; Smith, D. M. *J. Chem. Theory Comput.* **2008**, *4*, 1788.
- (38) Sun, Q.; Nelson, H.; Ly, T.; Stoltz, B. M.; Julian, R. R. *J. Proteome Res.* **2008**, *8*, 958.
- (39) Yang, Z.; Lam, C.; Chu, I. K.; Laskin, J. *J. Phys. Chem. B* **2008**, *112*, 12468.
- (40) Siu, C. K.; Ke, Y.; Orlova, G.; Hopkinson, A. C.; Siu, K. W. M. *J. Am. Soc. Mass Spectrom.* **2008**, *19*, 1799.
- (41) Wee, S.; Mortimer, A.; Moran, D.; Wright, A.; Barlow, C. K.; O'Hair, R. A. J.; Radom, L.; Easton, C. *J. Chem. Commun.* **2006**, 4233.
- (42) Pingitore, F.; Bleiholder, C.; Paizs, B.; Wesdemiotis, C. *Int. J. Mass Spectrom.* **2007**, *265*, 251.
- (43) Chu, I. K.; Zhao, J.; Xu, M.; Siu, S. O.; Hopkinson, A. C.; Siu, K. W. M. *J. Am. Chem. Soc.* **2008**, *130*, 7862.
- (44) Siu, C. K.; Zhao, J. F.; Laskin, J.; Chu, I. K.; Hopkinson, A. C.; Siu, K. W. M. *J. Am. Soc. Mass Spectrom.* **2009**, *20*, 996.
- (45) Rodriguez, C. F.; Cunje, A.; Shoeib, T.; Chu, I. K.; Hopkinson, A. C.; Siu, K. W. M. *J. Am. Chem. Soc.* **2001**, *123*, 3006.
- (46) Because reliable ionization energies are not available for all of the tripeptides GGX, we estimated these values by comparison with the ionization energies of the side chains provided in NIST-evaluated data. See: Hunter, E. P.; Lias, S. G. *NIST Chemistry WebBook*; <http://webbook.nist.gov/chemistry>.
- (47) Ke, Y.; Zhao, J.; Verkerk, U. H.; Hopkinson, A. C.; Siu, K. W. M. *J. Phys. Chem. B* **2007**, *111*, 14318.
- (48) Chan, W. C.; White, P. D. *Fmoc Solid Phase Peptide Synthesis: A Practical Approach*; Oxford: New York, 2000.
- (49) Henke, W.; Kremer, S.; Reinen, D. *Inorg. Chem.* **1983**, *22*, 2858.
- (50) Varkey, S. P.; Ratnasamy, C.; Ratnasamy, P. *J. Mol. Catal. A* **1998**, *135*, 295.
- (51) (a) Baer, T.; Hase, W. L. *Unimolecular Reaction Dynamics: Theory and Experiments*; Oxford: New York, 1996; p 188. (b) Baer, T.; Mayer, P. M. *J. Am. Soc. Mass Spectrom.* **1997**, *8*, 103.
- (52) Beyer, T.; Swinehart, D. F. *Commun. ACM* **1973**, *16*, 379.
- (53) SPARTAN, '04 Essential V2.0.0; Wavefunction, Inc.: Irvine, CA, 2004.
- (54) Frisch, M. J.; Trucks, G. W.; Schlegel, H. B.; Scuseria, G. E.; Robb, M. A.; Cheeseman, J. R.; Montgomery, J. A., Jr.; Vreven, T.; Kudin, K. N.; Burant, J. C.; Millam, J. M.; Iyengar, S. S.; Tomasi, J.; Barone, V.; Mennucci, B.; Cossi, M.; Scalmani, G.; Rega, N.; Petersson, G. A.; Nakatsuji, H.; Hada, M.; Ehara, M.; Toyota, K.; Fukuda, R.; Hasegawa, J.; Ishida, M.; Nakajima, T.; Honda, Y.; Kitao, O.; Nakai, H.; Klene, M.; Li, X.; Knox, J. E.; Hratchian, H. P.; Cross, J. B.; Bakken, V.; Adamo, C.; Jaramillo, J.; Gomperts, R.; Stratmann, R. E.; Yazyev, O.; Austin, A. J.; Cammi, R.; Pomelli, C.; Ochterski, J. W.; Ayala, P. Y.; Morokuma, K.; Voth, G. A.; Salvador, P.; Dannenberg, J. J.; Zakrzewski, V. G.; Dapprich, S.; Daniels, A. D.; Strain, M. C.; Farkas, O.; Malick, D. K.; Rabuck, A. D.; Raghavachari, K.; Foresman, J. B.; Ortiz, J. V.; Cui, Q.; Baboul, A. G.; Clifford, S.; Cioslowski, J.; Stefanov, B. B.; Liu, G.; Liashenko, A.; Piskorz, P.; Komaromi, I.; Martin, R. L.; Fox, D. J.; Keith, T.; Al-Laham, M. A.; Peng, C. Y.; Nanayakkara, A.; Challacombe, M.; Gill, P. M. W.; Johnson, B.; Chen, W.; Wong, M. W.; Gonzalez, C.; Pople, J. A. *Gaussian 03*, revision C.02; Gaussian, Inc.: Wallingford, CT, 2004.

JP908599A